Modelling and simulation of rack-pinion steering systems with manufacturing errors for performance prediction

Davide Marano* and Francesco Pellicano

Ferrari S.p.A.,
Maranello (MO), Italy
and
Dipartimento di Ingegneria 'Enzo Ferrari',
Universita' degli studi di Modena e Reggio Emilia,
MO, Italy
Email: davide.marano@ferrari.com
Email: davide.marano@unimore.it
Email: francesco.pellicano@unimore.it
*Corresponding author

Emanuele Pallara, Angelo Piantoni, Luca Tabaglio, Marco Lucchi and Stefano Orlandi

ZF-TRW Automotive Italia,
Via Valtrompia 125, Gardone VT (BS), Italy
Email: emanuele.pallara@altran.com
Email: angelo.piantoni@zf.com
Email: luca.tabaglio@zf.com
Email: marco.lucchi@zf.com
Email: stefano.orlandi@zf.com

Abstract: In the present paper, the modelling and simulation of a mechanical rack-and-pinion steering gear are presented. The study is performed using multibody simulations that include a reverse geometry rack to predict the functional measurements of the gear. A novel test for the characterisation of the functional performances of a mechanical steering gear is introduced and experimental data are used to validate prediction models.

Keywords: steering system; rack-and-pinion; multibody modelling; functional reverse.

Reference to this paper should be made as follows: Marano, D., Pellicano, F., Pallara, E., Piantoni, A., Tabaglio, L., Lucchi, M. and Orlandi, S. (2018) 'Modelling and simulation of rack-pinion steering systems with manufacturing errors for performance prediction', *Int. J. Vehicle Systems Modelling and Testing*, Vol. 13, No. 2, pp.178–198.

Biographical notes: Davide Marano received his Master's in Mechatronics in 2015 from the University of Catania. After graduation he worked as a Industrial PhD student for ZF Steering division. He currently works as a Powertrain Dynamics R&D Engineer in Ferrari Simulation and Know-How Department. His research interests include gear dynamics and powertrain NVH.

Francesco Pellicano received his MS in Aeronautical Engineering in 1992 and PhD in Theoretical and Applied Mechanics in 1996, University of Rome 'La Sapienza', Department of Mechanics and Aeronautics. He is currently a Full Professor at University of Modena and Reggio Emili and co-founder of Pulsar Dynamics.

Emanuele Pallara received his Mechanical Engineering from the Univerity of Salento in 2014. He currently works as a R&D Engineer in ZF Steering Division on behalf of Altran Italia.

Angelo Piantoni received his Master's degree in Mechanical Engineering from University of Brescia in 2011. In the same year, he joined ZF Steering Division initially as a University Researcher on friction, tribology and surface finish of steering gears and from 2012 as R&D Engineer. He is currently working as core engineering team lead for mechanical steering gears and part of ZF Global Rack and Pinion team.

Luca Tabaglio holds a Master degree in Mechanical Engineering from University of Brescia in 2003. After one year of University Research he joined TRW in Steering System Engineering Department. He covered different roles in TRW / ZF as Product Engineer and R&D Team Leader. He is currently appointed as the MSG Design Manager for Global Mechanical Steering Gear Systems for ZF Division A – Active & Passive Safety.

Marco Lucchi holds a Mechanical Engineering Master degree in 1996 from University of Brescia. After a couple of years spent in the research area of metal forming and cutting processes simulations at Ohio State University and University of Brescia, his working experiences has been in automotive companies, mostly in TRW & ZF covering various roles in product and process engineering.

Stefano Orlandi holds a Master degree in Mechanical Engineering from University of Brescia in 2001 and an Executive MBA from MIP Politecnico di Milano Graduate School of Business in 2018. He covered different roles in TRW/ZF as Product Engineer, Continuous Improvement Manager and Operations Manager of ZF Gardone plant in Italy. He is currently appointed as a Chief Engineer for ZF Division A – Active & Passive Safety.

This paper is a revised and expanded version of a paper entitled 'Effects of gear manufacturing errors on rack-and-pinion steering meshing' presented at the First World Congress on Condition Monitoring, London, 13–16 June 2017.

1 Introduction

The purpose of the steering system is to provide the driver with control of lateral vehicle dynamics. Standard designs of mechanical steering systems are rack-and-pinion steering (RPS) and recirculating ball steering (Figure 1).

Figure 1 Classification of steering system design

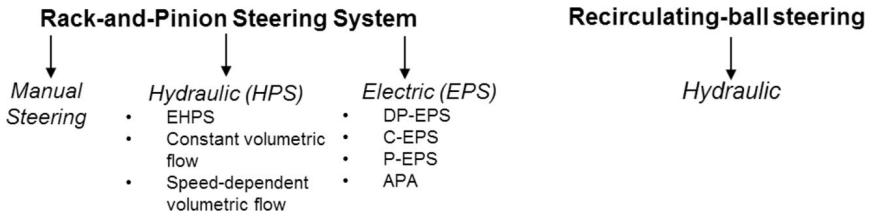

In a manual RPS system, the turning of the steering wheel is transformed in rack shift and rack force by the dovetailing components, i.e., pinion and rack; the system is operated only by the driver's arms on the steering wheel. The increase of vehicles' weight, and the need of improved vehicle steerability have led to the development of power steering. The actual technologies include hydraulic power steering (HPS), electro-hydraulic power steering (EHPS), and electromechanical electric power steering (EPS) steering power support. In HPS the supporting power is provided by a volume flow, usually generated by a vane pump driven by the internal combustion engine (ICE). In EHPS a pump operating independently of the ICE is used. In electrically assisted systems (EPS) the supporting power is generated by an electric motor, powered through the electrical system on board (Figure 2). In Dawane (2010) and Xue and Watton (2005) a model of power steering system and hydraulic power steering system is presented. Details on steering systems design can be found in Harrer and Pfeffer (2016).

Figure 2 Column drive EPS

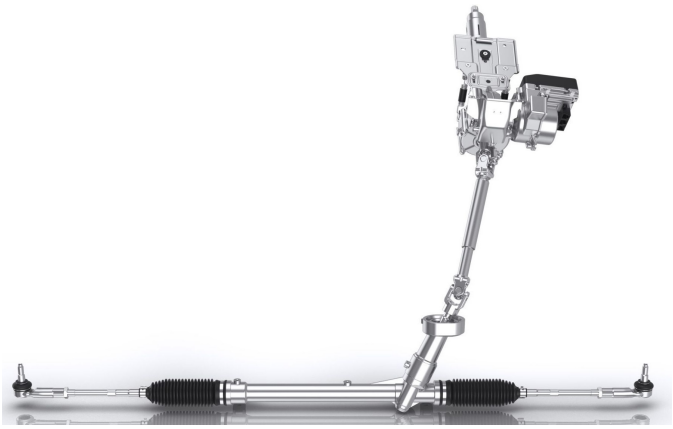

Source: Courtesy of ZF Group

The literature on steering systems is generally focused on kinematic analysis and synthesis of linkage systems (see, e.g., Yao and Angeles, 2000; Simionescu and Smith, 2000).

RPS design and manufacturing have been studied in Bishop and Baxter (1984) and a model of mesh friction and mechanical efficiency of RPS system was proposed in Wou et al. (2001). A multibody model of RPS system was proposed in Kamble et al. (2004) and Kamble and Saha (2005) for virtual prototyping; some of the gear manufacturing and assembly errors were considered in the model proposed in Kamble and Saha (2007).

Gear contact modelling in the presence of errors has been focused on both numerical and analytical methods. In Litvin and Fuentes (2004) an analytical formulation for the crossed helical pinion and rack kinematics is developed. The effects of machining errors, assembly errors and tooth modifications on loading capacity, load-sharing ratio and transmission error of a pair of spur gears have been quantitatively investigated using finite element method software by Li (2007). Indexing errors are a cause of significant vibration and overloading in geared systems; in Spitas and Spitas (2006) a single-stage spur gear is dynamically simulated using various scenarios of error distribution and profile corrections, to calculate the overload factor. An analytical approach for the analysis of tooth contact and load distribution of helical gears with crossed axis is proposed by Zhang and Fang (1999); this approach is based on a tooth contact model that accommodates the influence of tooth profile modifications, gear manufacturing errors and tooth surface deformation on gear mesh quality. Chen and Shao (2013) have proposed a general analytical mesh stiffness model to include the effect of the gear tooth errors. The influence of gear manufacturing errors on rack and helical pinion meshing has been extensively studied by Marano et al. (2017) with analytical and numerical solution.

Literature on multibody simulation of steering systems, to the best of the authors' knowledge, does not report analysis with real gear geometry, obtained by coordinate measuring machine (CMM) measurements. The aim of the present paper is to estimate the mechanical rack-and-pinion gear functional behaviour by means of a multibody simulation of the system considering measured rack-and-pinion gear geometry. Reverse engineering is performed by CMM measurement to obtain the rack geometry, and a compliant contact force model is used in the simulation.

Standard functional test of mechanical steering gears, to evaluate the performance of the gear meshing, is reported in Harrer and Pfeffer (2016) and described in Section 3. A new functional test, named rack rolling, is proposed in the present paper and implemented by means of a new test bench to evaluate the rack-and-pinion meshing quality. A simplified analytical model is proposed to estimate the rack rolling as a function of gear manufacturing errors. Multibody and analytical models are validated through experimental measurements, resulting in good agreement.

2 Main components of a mechanical rack-and-pinion gear

The present paper deals with RPS systems. In the following the steering system is described in detail. A typical rack-and-pinion system is shown in Figure 3: the gear housing (Figure 3 element 1) supports all the components of the steering gear, it can be either rigidly or elastically mounted on the vehicle chassis through elastic joints. The steering pinion (Figure 3 element 2) is connected to the column and wheel by the

intermediate steering shaft, and it is meshing with the rack bar (Figure 3 element 3) teeth. The movement of the rack bar with respect to the housing is supported and guided by the yoke assembly (Figure 3 element 4) and a bushing (Figure 3 element 5); the linear rack motion is transmitted to the wheel carrier via the tie rods with its ball joints (Figure 3 element 6).

Figure 3 RPS system

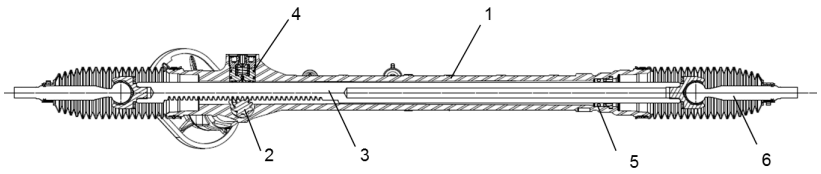

A detail of the rack yoke assembly is shown in Figure 4.

Figure 4 Rack yoke assembly detail

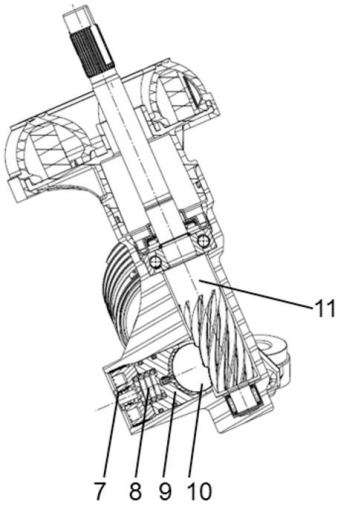

In order to guarantee zero backlash meshing the rack bar (Figure 4 element 10) is preloaded against the pinion (Figure 4 element 11) by a spring-loaded rack yoke (Figure 4 element 9). The spring (Figure 4 element 8) preload can be set by an adjuster bolt (Figure 4 element 7). The zero backlash condition is required to optimise steering feeling and NVH performances.

3 Functional requirements of a mechanical rack gear

Functional performances of a mechanical steering gear are assessed by specific tests; all tests are carried out at a gear without tie rods in built-in position at controlled room temperature. A functional scheme of the adopted test bench is represented in Figure 5.

A linear drive is attached to the rack strainlessly, no additional loads are applied at the input shaft, so that the shaft moves freely when the rack is shifted with a constant speed of 5–10 mm/s, as reported in Harrer and Pfeffer (2016). The main functional tests are: rack yoke clearance; rack displacement force; steering pinion torque. A new test, named rack rolling, is proposed in the following.

Figure 5 Rack gear test bench (see online version for colours)

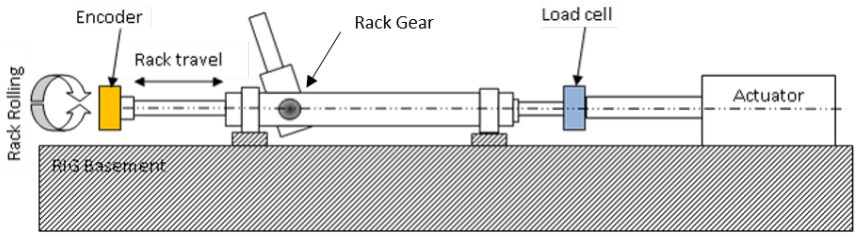

3.1 Rack yoke clearance test rig

Owing to gear manufacturing errors, the centre distance of the rack pinion meshing is variable, as explained in Marano et al. (2017); a proper rack yoke clearance is thus set during assembly process. If the clearance is very small, then a bigger friction at the gear mesh is expected; conversely, if the highest limitation of the clearance is exceeded, there is risk of steering rattle noise. The yoke clearance test is performed as shown in Figure 6, actuating the rack and recording the yoke position as a function of rack axial position by means of a linear transducer; gyroscopic yoke movements are not detected. As reported in Harrer and Pfeffer (2016), a limitation of highest rack yoke clearance is fixed (e.g., 100 μm) to control the friction and noise response of the rack-and-pinion gear.

Figure 6 Yoke clearance test

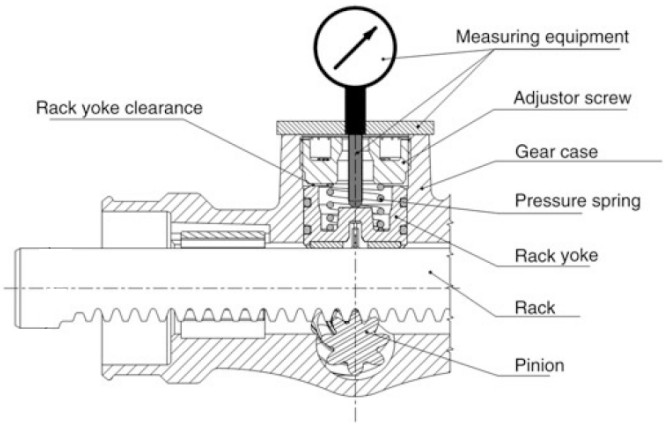

3.2 Rack displacement force

The rack displacement force test is performed by attaching a linear drive to the rack with no additional loads at the input shaft, so that the shaft freely moves when the rack is shifted. The rack displacement and the rack force are recorded over the measuring cycle. Rack force is function of rack yoke preload, lubrication and surface conditions as well as gear mesh geometry. As reported in Harrer and Pfeffer (2016), rack forces of 150–350 N are admissible.

3.3 Steering pinion torque test

The steering pinion torque test is carried out by imposing a rotation to the input shaft with constant velocity; no loading elements are applied to the rack, so that it moves freely. The torque at the input shaft and the rotation angle are recorded over a measuring cycle. As reported in Harrer and Pfeffer (2016), typical values of the pinion torque are in the range of 0.8–2.0 Nm.

3.4 Rack rolling

The mechanical steering system is often designed in such a way that the rack-and-pinion axes are not perpendicular. The skew axis meshing gives rise to sliding, which creates a torque tending to rotate the rack bar. Since the rack torque depends on the rack-and-pinion mesh design and manufacturing errors, the rack bar rotation generated during the meshing measured without applied load can be considered as a meshing quality measurable. The rack rolling is recorded as a function of the rack axial position by means of a high resolution rotary encoder.

4 Multibody modelling

In the following, the multibody modelling of the system is explained. The model is realised by means of FunctionBay RecurDyn®(multi-body dynamics software based on recursive formulation). In RPS gear, the rack is supported by a a flexible bush at one end and by a yoke (Figure 7), preloaded by a spring, at the other end. This arrangement compensates both for slight misalignments of rack axis and centre distance variation due to gear manufacturing errors. The pinion is assembled within the housing with bearings, thus having fixed axis of revolution. The kinematic model proposed in here aims to replicate the real RPS behaviour.

Figure 7 Kinematic model of the system (see online version for colours)

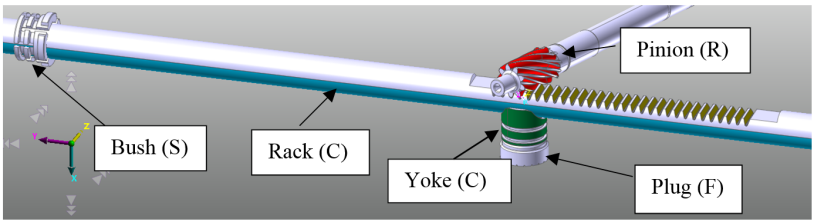

The rack geometry is inspected by means of a coordinate measuring machine (Zeiss Contura©CMM). The detected parameters are: helix and pressure angles, transverse pitch and overoller measurement (ISO BS. 21771, 2007); rack teeth flank planarity is checked. A parametric CAD model is created to reproduce the real rack geometry: from the CMM readings, the software creates the rack teeth planes and a volume of the rack is obtained by filling in the surfaces. Each joint requires the definition of a base body and an action body, to constrain their relative coordinates, velocities and accelerations, as explained in FunctionBay (2012); constraints are listed in Table 1.

Table 1 Multibody model constraints

Reference body	*Action body*	*Joint*
Ground	Pinion	Revolute R
Ground	Bush	Bushing (S)
Bush	Rack	Cylindrical (C)
Ground	Yoke	Cylindrical (C)
Ground	Plug	Fixed (F)
Liner	Yoke	Fixed (F)

Figure 8 Rack-and-pinion contact discretisaion (see online version for colours)

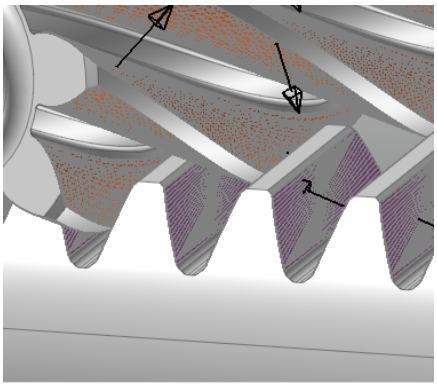

4.1 Contact setting

An overview of the state of the art on contact modelling methodologies is provided in Gilardi and Sharf (2002). A robust contact algorithm for a compliant contact force model between bodies of complex geometry is implemented in the software Recurdyn®, as explained in FunctionBay (2012) and Choi et al. (2010). Via this approach, surfaces are represented using triangular patches: the boundary of the pinion teeth and the flanks of rack teeth are approximated by triangular patches, as shown in Figure 8. The normal contact force is calculated as a function of the penetration, say δ of the pinion tooth flank nodes into the rack flank patch as follows:

$$f_n = K\delta^a + C\frac{\dot{\delta}}{|\dot{\delta}|}|\dot{\delta}|^b\delta^c$$

where $\dot{\delta}$ is the time derivative of δ, K and C are the spring and damping coefficients, which are determined by an experimental method as explained in Machado et al. (2012) and Flores and Lankarani (2016). The exponents a and b, generate a non-linear contact force while the exponent c yields an indentation damping effect. When the penetration is very small, the contact force may be negative due to a negative damping force; this situation can be overcome by using the indentation exponent greater than one. The results from Hertzian contact theory are used to model the contact stiffness, as explained in Popov (2010); contact parameters adopted in simulation are listed in Table 2.

Table 2 Multibody contact parameters

Interface	*K [N/mm]*	*C [Ns/mm]*	*a*	*b*	*c*
Rack-pinion	3.45 E6	0.1	1	0	0
Rack-yoke liner	1.44 E6	0.1	1.5	0	0
Yoke-plug	1 E8	0.1	1.5	0	0

4.2 Surface patch

The contact surface discretisation is controlled by the maximum facet size facto. This parameter sets the maximum length of facets on the surfaces of the contact bodies. For efficiency, the solver partitions the surfaces of the contact bodies into small, triangular surface facets. A smaller value creates more facets, which increases precision in the contact solution. The maximum step size factor reduces the integrator maximum step size temporarily, as the action body approaches the base body during the contact portion of the simulation. A larger maximum step size factor results in smaller step sizes, which provide greater solver precision. Patch parameters are set as in Table 3.

Table 3 Multibody contact parameters

Patch parameter	*Rack*	*Pinion*	*Liner*	*Yoke*	*Plug*
Surface type	Triangle	Triangle	Triangle	Triangle	Triangle
Plane tolerance factor	3	0.5	3	3	3
Max facet size factor	2	0.1	2	2	2

4.3 Friction setting

The main contributions to the friction come from the components affected by sliding on their surfaces, as explained in Gritti et al. (2017) and Wou et al. (2001). The rack bush contribution depends on the geometrical characteristics, lubrication condition and material. The sliding force can be considered constant and independent from the other friction sources. The yoke liner contribution depends on the material (friction coefficient), geometrical characteristics and yoke spring preload. The higher friction contribution is given by the gear meshing. During the motion there are many sliding surfaces which dissipate energy; the friction force depends on gear parameters, teeth surface roughness, yoke spring load and lubrication conditions. All of these contributions are speed dependent.

Figure 9 Perfect rack-pinion meshing (see online version for colours)

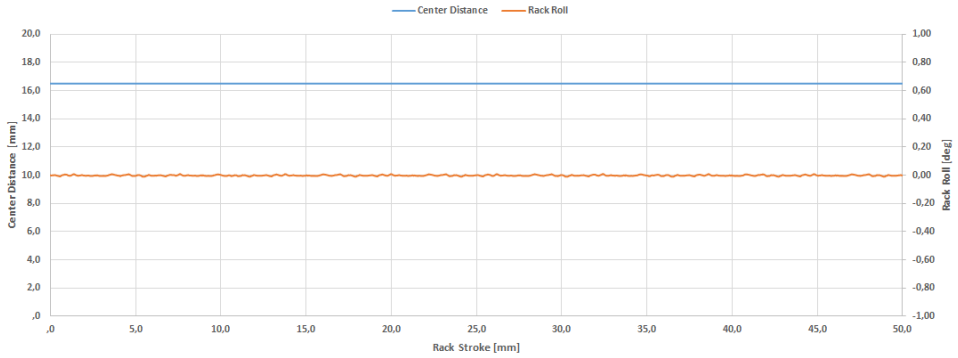

4.4 Model benchmark

In order to validate the results of multibody model, a benchmark of a numerical solution of a perfect rack-pinion system is proposed in the following. Contact parameters, surface patch and friction have been set as reported in Tables 2 and 3. As shown in Figure 9, centre distance variation and rack roll are negligible and simulation results are very stable.

5 Analytical model

5.1 Roll angle estimation

The rack rolling angle due to rack geometrical errors is estimated by a simplified analytical model, as explained in the following. Assembly/alignment errors and pinion geometrical imperfections are neglected.

The transverse (normal) section coordinate-system model is shown in Figures 10 and 11, where y (y') is the longitudinal rack axis, z (z') is the transverse axis and x (x') axis is obtained according to the right-hand rule.

$$\vec{n}'^{R} = -\cos(\alpha_n^R)\cdot\hat{j}' + \sin(\alpha_n^R)\cdot\hat{k}'$$
$$\vec{n}'^{L} = +\cos(\alpha_n^L)\cdot\hat{j}' + \sin(\alpha_n^L)\cdot\hat{k}'$$

where α_n^L (resp., α_n^R) is the left (resp., right) normal pressure angle and ($\hat{i}$, $\hat{j}$, $\hat{k}$) are unit vectors. Vectors $\vec{n}^R$ and $\vec{n}^L$, in transverse plane, can be obtained rotating $\vec{n}'^{R}$ and $\vec{n}'^{L}$, respectively, by β^R and β^L, around z axis, giving:

$$\vec{n}^R = \begin{bmatrix} \cos\beta^R & \sin\beta^R & 0 \\ -\sin\beta^R & \cos\beta^R & 0 \\ 0 & 0 & 1 \end{bmatrix} \cdot \begin{bmatrix} 0 \\ -\cos\alpha_n^R \\ \sin\alpha_n^R \end{bmatrix} = \begin{bmatrix} -\cos\alpha_n^R \sin\beta^R \\ -\cos\alpha_n^R \cos\beta^R \\ \sin\alpha_n^R \end{bmatrix} = \begin{bmatrix} a^R \\ b^R \\ c^R \end{bmatrix} \quad (1)$$

$$\vec{n}^L = \begin{bmatrix} \cos\beta^L & \sin\beta^L & 0 \\ -\sin\beta^L & \cos\beta^L & 0 \\ 0 & 0 & 1 \end{bmatrix} \cdot \begin{bmatrix} 0 \\ +\cos\alpha_n^L \\ \sin\alpha_n^L \end{bmatrix} = \begin{bmatrix} +\cos\alpha_n^L \sin\beta^L \\ +\cos\alpha_n^L \cos\beta^L \\ \sin\alpha_n^L \end{bmatrix} = \begin{bmatrix} a^L \\ b^L \\ c^L \end{bmatrix} \quad (2)$$

The rack flanks are thus determined in point-normal form, given the normal vectors $\overrightarrow{n^R}$ and $\overrightarrow{n^L}$ to right and left flank and points P_R and P_L, respectively, belonging to right and left flank:

$$\begin{cases} P_R = (x_0^R; y_0^R; z_0^R) = (0; +e_t/2; \text{BRTR} + h_f - D_r/2); \\ P_L = (x_0^L; y_0^L; z_0^L) = (0; -e_t/2; \text{BRTR} + h_f - D_r/2) \end{cases} \tag{3}$$

where BRTR is the back of rack to tooth root distance, D_r is the rack diameter, e_t is the transverse spacewidth and h_f is the rack dedendum according to ISO BS. 21771 (2007).

Figure 10 Coordinate-system, 1: transverse section, 2: normal section

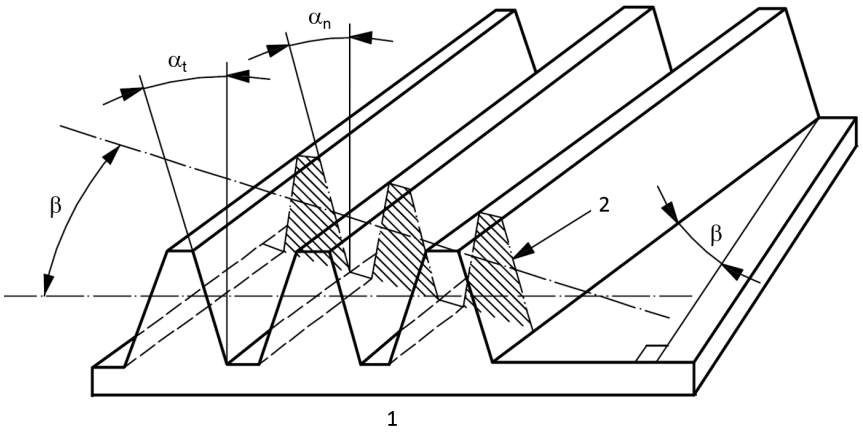

Figure 11 Coordinate-system, transverse section (see online version for colours)

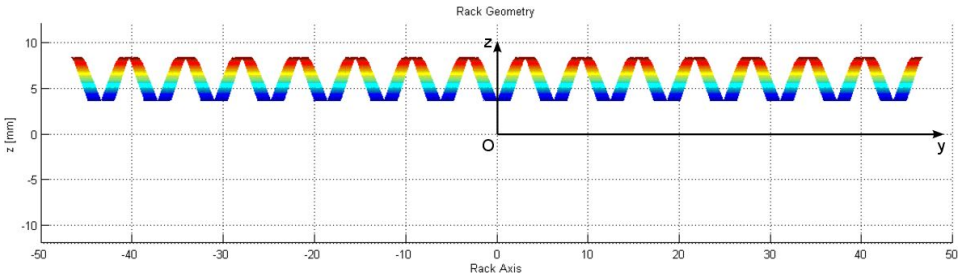

Let us define a parametric cylinder T with axis parallel to $\vec{x}$ and centre $(0,\ 0,\ z_0)$ as follows:

$$\begin{bmatrix} x_{cyl} \\ y_{cyl} \\ z_{cyl} \end{bmatrix} = \begin{bmatrix} +\cos\varphi & 0 & +\sin\varphi \\ 0 & 1 & 0 \\ -\sin\varphi & 0 & +\cos\varphi \end{bmatrix} \begin{bmatrix} +\cos\gamma & +\sin\gamma & 0 \\ -\sin\gamma & +\cos\gamma & 0 \\ 0 & 0 & 1 \end{bmatrix} \cdot \begin{bmatrix} t \\ (D_M \cdot \cos\theta)/2 \\ z_c + (D_M \cdot \sin\theta)/2 \end{bmatrix} \tag{4}$$

where φ is the roll angle ($\vec{y}$ axis), γ is the yaw angle ($\vec{z}$ axis) and D_M is the cylinder diameter. Developing equation (4) one obtains:

$$\begin{cases} x_{cyl} = \sin\varphi(z_c + r\sin\theta) + t\cos\gamma\cos\varphi + r\cos\varphi\cos\theta\sin\gamma; \\ y_{cyl} = -t\sin\gamma + r\cos\gamma\cos\theta; \\ z_{cyl} = \cos\varphi(z_c + r\sin\theta) - t\cos\gamma\sin\varphi - r\cos\theta\sin\gamma\sin\varphi; \end{cases} \tag{5}$$

The equation of the tangent plane to the above cylinder at a point $(x_0,\ y_0,\ z_0)$ is obtained by imposing:

$$\det\begin{bmatrix} x - x_0 & y - y_0 & z - z_0 \\ \partial x_{cyl}/\partial t & \partial y_{cyl}/\partial t & \partial z_{cyl}/\partial t \\ \partial x_{cyl}/\partial\theta & \partial y_{cyl}/\partial\theta & \partial z_{cyl}/\partial\theta \end{bmatrix} = 0 \tag{6}$$

which leads to:

$$\begin{cases} a_T = -r(\sin\varphi\sin\theta + \cos\varphi\cos\theta\sin\gamma); \\ b_T = -r\cos\theta\cos\gamma; \\ c_T = r(\cos\theta\sin\gamma\sin\varphi - \sin\theta\cos\varphi); \\ d_T = r[x_0(\sin\theta\sin\varphi + \cos\theta\cos\varphi\sin\gamma) \\ +y_0\cos\theta\cos\gamma - z_0(\cos\theta\sin\varphi\sin\gamma - \sin\theta\cos\varphi)]. \end{cases} \tag{7}$$

Assuming φ small enough and dividing by $-r$, equation (7) becomes:

$$\begin{cases} a_T = \varphi\sin\theta + \cos\theta\sin\gamma; \\ b_T = \cos\theta\cos\gamma; \\ c_T = \sin\theta - \varphi\cos\theta\sin\gamma; \\ d_T = -x_0(\varphi\sin\theta + \cos\theta\sin\gamma) - y_0\cos\theta\cos\gamma + z_0(\cos\theta\varphi\sin\gamma - \sin\theta); \end{cases} \tag{8}$$

T is tangent to the right vane flank if:

$$\begin{cases} a_T = a^R; \\ b_T = b^R; \\ c_T = c^R; \\ d_T = d^R. \end{cases} \tag{9}$$

leading to:

$$\begin{cases} \varphi\sin\theta^R + \cos\theta^R\sin\gamma = -\cos\alpha_n^R\sin\beta^R; \\ \cos\theta^R\cos\gamma = -\cos\alpha_n^R\cos\beta^R; \\ \sin\theta^R - \varphi\cos\theta^R\sin\gamma = \sin\alpha_n^R; \\ -x_0^R(\varphi\sin\theta^R + \cos\theta^R\sin\gamma) - y_0^R\cos\theta^R cos\gamma \\ +z_0^R(\varphi\cos\theta^R\sin\gamma - \sin\theta^R) = \\ = \cos\alpha_n^R\cos\beta^R e_t/2 - (BRTR + h_r - D_r/2)\sin\alpha_n^R \end{cases} \tag{10}$$

$$\begin{cases} \varphi \sin\theta^L + \cos\theta^L \sin\gamma = +\cos\alpha_n^L \sin\beta^L; \\ \cos\theta^L \cos\gamma = +\cos\alpha_n^L \cos\beta^L; \\ \sin\theta^L - \varphi\cos\theta^L \sin\gamma = \sin\alpha_n^L; \\ -x_0^L(\varphi\sin\theta^L + \cos\theta^L \sin\gamma) - y_0^L \cos\theta^L cos\gamma \\ +z_0^L(\varphi\cos\theta^L \sin\gamma - \sin\theta^L) = \\ = \cos\alpha_n^L \cos\beta^L e_t/2 - (BRTR + h_r - D_r/2)\sin\alpha_n^L \end{cases} \tag{11}$$

Imposing the tangency of the cylinder T with both left and right vane flanks one arrives at:

$$\begin{cases} \tan\beta^L = \dfrac{\varphi\tan\theta^L}{\cos\gamma} + \tan\gamma \\ \tan\beta^R = \dfrac{\varphi\tan\theta^R}{\cos\gamma} + \tan\gamma \end{cases} \tag{12}$$

$$\begin{cases} +\dfrac{\tan\alpha_n^L}{\cos\beta^L} = \dfrac{\tan\theta^L}{\cos\gamma} - \varphi\tan\gamma \\ -\dfrac{\tan\alpha_n^R}{\cos\beta^R} = \dfrac{\tan\theta^R}{\cos\gamma} - \varphi\tan\gamma \end{cases} \tag{13}$$

Subtracting term by term equation (12) and equation (13) provides

$$\begin{cases} \tan\beta^R - \tan\beta^L = \dfrac{\varphi}{\cos\gamma}(\tan\theta^R - \tan\theta^L); \\ \varphi = -\dfrac{\tan\beta^R - \tan\beta^L}{\tan\alpha_n^R/\cos\beta^R + \tan\alpha_n^L/\cos\beta^L} \end{cases} \tag{14}$$

The roll and yaw angles are achieved with simple algebraic computation, giving:

$$\begin{cases} \varphi & \approx -\dfrac{\beta^R - \beta^L}{(\tan\alpha_n^R + \tan\alpha_n^L)\cdot\cos\beta} \\ \tan\gamma & \approx \tan(\dfrac{\beta^R + \beta^L}{2}) \end{cases} \tag{15}$$

The angles φ and γ are calculated for each rack spacewidth according to CMM measurement; the rack rolling estimation is obtained by a linear interpolation of the calculated values.

5.2 Centre distance variation estimation

The centre distance variation is calculated as a function of CMM measurements. For the sake of completeness, the theory to estimate the operating centre distance developed in Marano et al. (2017) is reported below. The geometrical errors of rack gear are shortly listed and the contribution of each error on centre distance variation is analytically estimated.

5.2.1 Over roller error

The rack is measured by means of a spherical probe placed successively in the tooth spaces. In measuring a rack, the pin is ideally tangent with the tooth flank at the pitch line; a variation of over pin measure is thus related to a pitch line shift. In the case of a helical rack, module m, and normal pressure angle α_n, the ideal pin diameter is given by:

$$d'_p = \frac{\pi m_n - s'}{\cos \alpha_n}$$

where s' is the rack tooth thickness. The ideal over pin measurement is given by:

$$M = K - \frac{\pi m_n - s'}{2 \tan \alpha_n} + \frac{d_p}{2}(1 + \frac{1}{\sin \alpha_n})$$

where d_p is the rounded value of calculated pin diameter, relevant dimensions are shown in Figure 12.

Figure 12 Over pin measurement for a rack using a pin or a ball

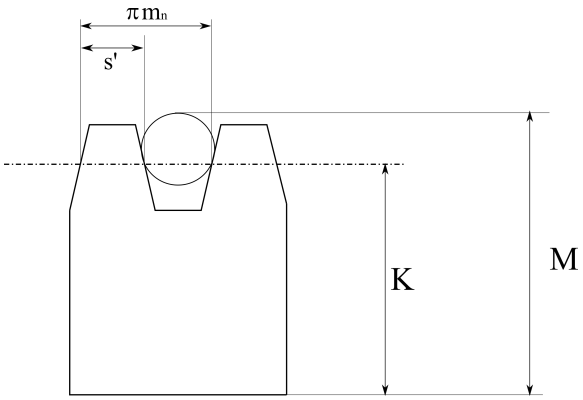

Figure 13 Pitch measurement for a rack using a pin or a ball

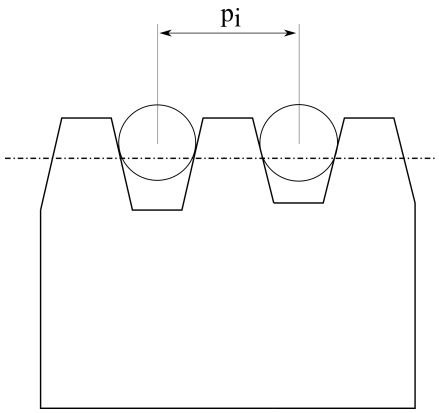

5.2.2 Pitch error

The axial pitch is measured inserting sequentially the pin in successive tooth spaces and calculating the axial distance between the two adjacent measured values; a deviation from the nominal pitch value is thus related to a variation of tooth width. A pitch error changes the centre distance of:

$$\Delta BC_{PitchError} = \frac{\Delta p_i}{2\tan\alpha_n}$$

5.2.3 Lead angle error

In Figure 14, a normal section to rack axis is shown; the nominal lead angle is denoted by β_{rack}, the rack facewidth by k. The effect of a lead angle error $\Delta\beta$ on the centre distance variation is given by:

$$\Delta BC_{LeadError} = \frac{k\tan(\Delta\beta)}{2\tan\alpha_n}$$

Figure 14 Rack lead angle error (see online version for colours)

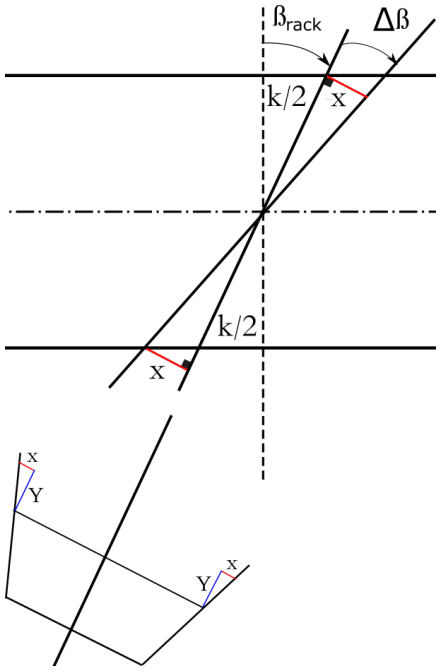

The operating centre distance can be calculated as:

$$\Delta CD = \frac{|\Delta p_i|}{2\tan\alpha_n} + \frac{K\tan(\Delta\beta_i)}{2\tan\alpha_n} + \Delta M_{rk}, \tag{16}$$

where Δp_i is the pitch error, $\Delta\beta_i$ is the lead angle error and ΔM_{rk} is the overoller error.

6 Experimental measurements

The rack rolling is recorded as a function of rack axial position by means of the experimental setup introduced in Section 3.4. The measurements are performed on two different gear sets, as presented in Table 4.

Table 4 Gear set design parameters

	Transverse pitch [mm]	*Pressure angle [deg]*	*Helix angle [deg]*
Gear set 1	6	20	5
Gear set 2	6.4	20	10

Figure 15 Gear set 1 – CMM measurements (see online version for colours)

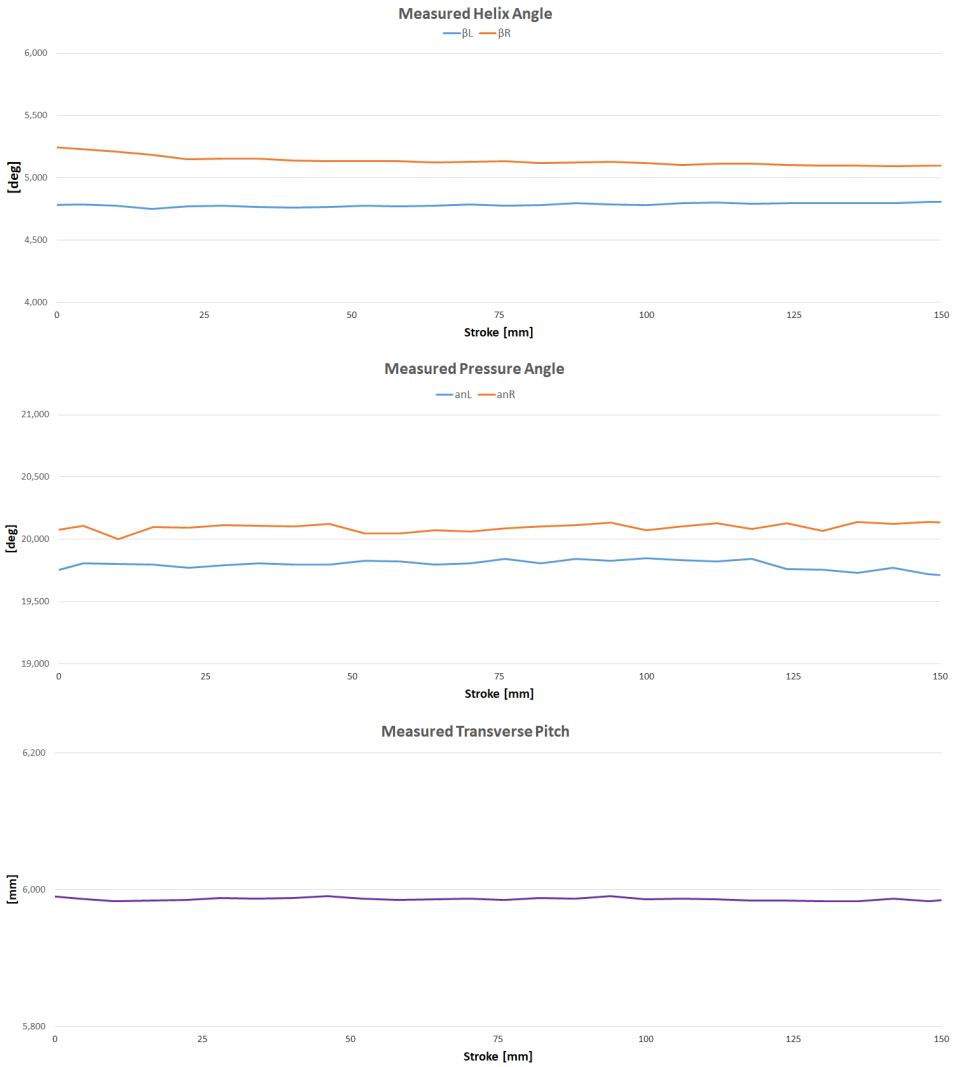

Both gear sets are measured by means of a CMM before the functional testing; helix angle, pressure angle and transverse pitch are reported respectively in Figure 15 for gear set 1 and Figure 16 for gear set 2. Measured gear errors can be attributed both to gear cut and heat treatment process.

Gear measurements are used to estimate rack rolling signal carrier and centre distance variation by means of the proposed analytical model and to generate gear CAD models for the multibody numerical simulation.

Figure 16 Gear set 2 – CMM measurements (see online version for colours)

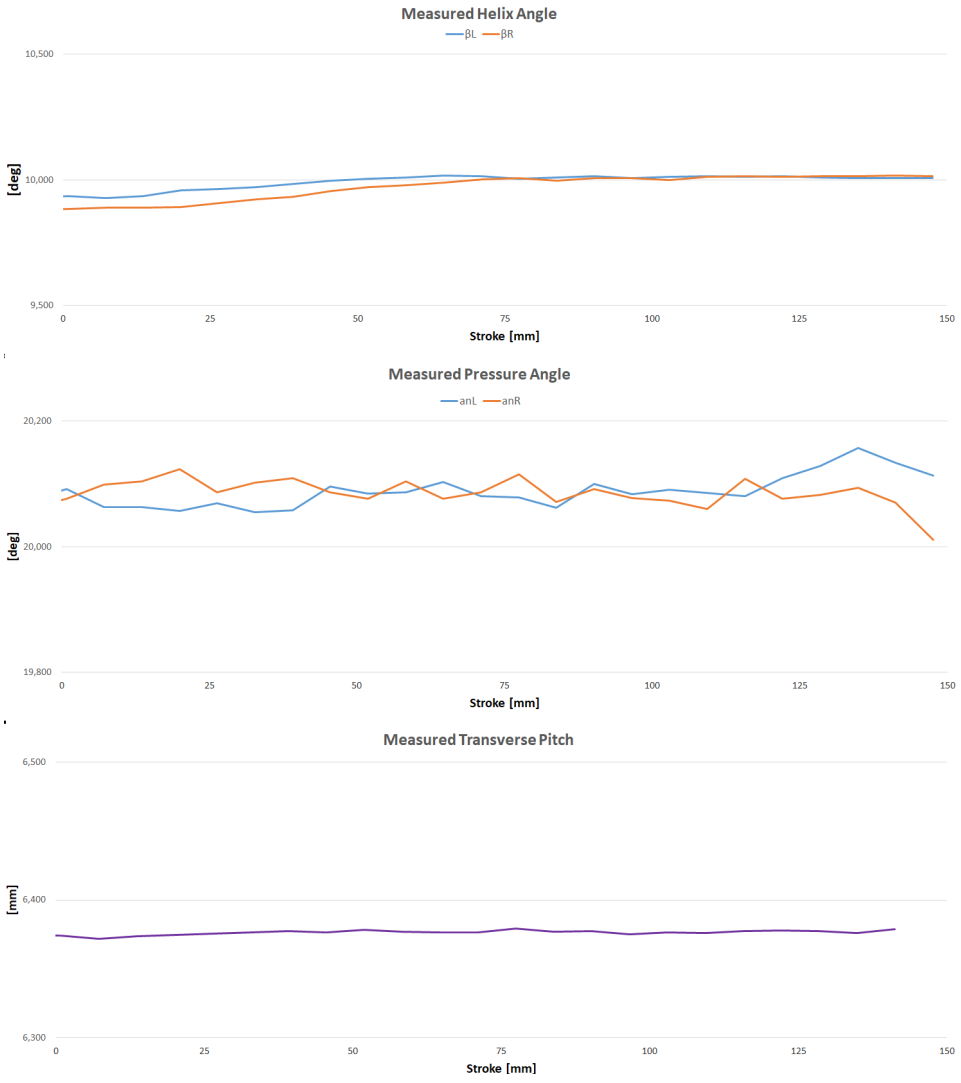

7 Results

The meshing centre distance variation is estimated by equation (16), and rack rolling carrier signal by equation (15) as a function of CMM gear measurements reported in the previous section. A multibody simulation is set as explained in Section 4 considering reverse geometry of rack. The rack rolling and the yoke clearance obtained analytically and numerically are compared in Figure 17 for gear set 1, and in Figure 18 for gear set 2.

The numeric model provides a good estimation of the rack bar movements within two consecutive rack vanes; differences between measured and simulated signal can be attributed to the pinion manufacturing errors, not considered in the present analysis.

Figure 17 Gear set 1 – rack rolling [mm] and yoke clearance [deg] test: experimental data (orange), multibody simulation (green), analytical estimation (blue) (see online version for colours)

Figure 18 Gear set 2 – rack rolling [mm] and yoke clearance [deg] test: experimental data (orange), multibody simulation (green), analytical estimation (blue) (see online version for colours)

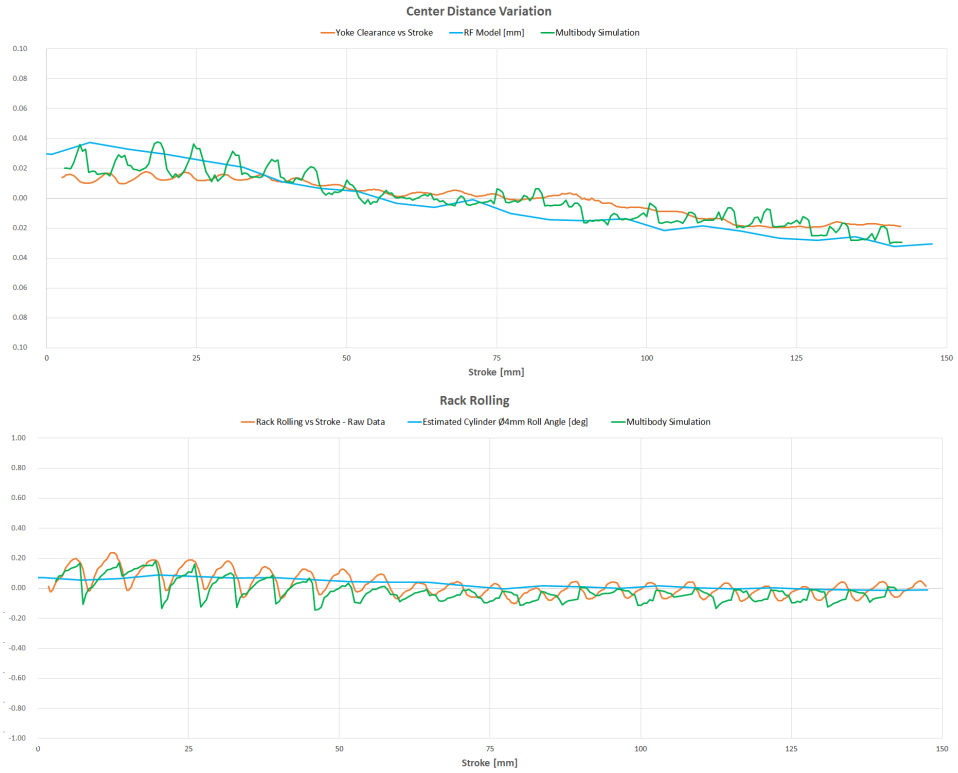

8 Conclusions

In the present paper a novel test for the characterisation of the functional performances of a mechanical steering gear is proposed. A concept test bench to measure the rack bar rotation during the rack-and-pinion meshing is proposed. A multi-body model is developed to estimate the functional behaviour of the rack-and-pinion gear. The numerical model shows good performance in terms of accuracy of results.

An analytical model is developed to estimate the rack roll as a function of measured rack manufacturing errors; it allows to obtain the trend through a simple closed form formulation.

The prediction of centre distance variation and rack rolling functional performances can be used during design phase in order to define the tolerance range for rack bar in terms of gear geometry accuracy class leading to customer specification compliance.

References

Bishop, A.E. and Baxter, J. (1984) *New Rack-and-pinion Steering Design and Manufacturing Technology*, No. 841199, SAE Technical Paper.

Chen, Z. and Shao, Y. (2013) 'Mesh stiffness calculation of a spur gear pair with tooth profile modification and tooth root crack', *Mechanism and Machine Theory*, Vol. 62, pp.63–74.

Choi, J., Ryu, H.S., Kim, C.W. and Choi, J.H. (2010) 'An efficient and robust contact algorithm for a compliant contact force model between bodies of complex geometry', *Multibody System Dynamics*, Vol. 23, No. 1, p.99.

Dawane, M. (2010) 'Modelling and analysis of power steering system', *International Journal of Electric and Hybrid Vehicles*, Vol. 2, No. 3, pp.211–221.

Flores, P. and Lankarani, H.M. (2016) *Contact Force Models for Multibody Dynamics*, Vol. 226, Springer.

FunctionBay, K.K. (2012) 'Recurdyn/solver theoretical manual', *Function-Bay*, pp.122–124.

Gilardi, G. and Sharf, I. (2002) 'Literature survey of contact dynamics modelling', *Mechanism and Machine Theory*, Vol. 37, No. 10, pp.1213–1239.

Gritti, G., Peverada, F., Orlandi, S., Gadola, M., Uberti, S., Chindamo, D. and Olivi, A. (2017) 'Mechanical steering gear internal friction: effects on the drive feel and development of an analytic experimental model for its prediction', *Advances on Mechanics, Design Engineering and Manufacturing*, pp.339–350, Springer, Cham.

Harrer, M. and Pfeffer, P. (Eds.) (2016) *Steering Handbook*, Springer.

ISO BS. 21771 (2007) *Gears-cylindrical Involute Gears and Gear Pairs-concepts and Geometry*.

Kamble, N. and Saha, S.K. (2005) *Effect of Pinion Profile Modification on Rack-and-pinion Steering Gear*, No. 2005-01-1273, SAE Technical Paper, pp.83–90.

Kamble, N. and Saha, S.K. (2006) 'Developing a virtual prototype of a rack-and-pinion steering system', *International Journal of Vehicle Systems Modelling and Testing*, Vol. 2, No. 1, pp.61–79.

Kamble, N., Marothiya, P., Saha, S.K., Priyadarshi, R., Deshmukh, K.M. and Rao, A.D. (2004) *Experimental Study of Torque Characteristics of Rack-and-Pinion Steering System*, No. 2004-28-0031, SAE Technical Paper.

Li, S. (2007) 'Effects of machining errors, assembly errors and tooth modifications on loading capacity, load-sharing ratio and transmission error of a pair of spur gears', *Mechanism and Machine Theory*, Vol. 42, No. 6, pp.698–726.

Litvin, F.L. and Fuentes, A. (2004) *Gear Geometry and Applied Theory*, Cambridge University Press.

Machado, M. et al. (2012) 'Compliant contact force models in multibody dynamics: evolution of the Hertz contact theory', *Mechanism and Machine Theory*, Vol. 53, pp.99–121.

Marano, D., Piantoni, A., Tabaglio, L., Lucchi, M., Barbieri, M. and Pellicano, F. (2017) 'Effects of gear manufacturing errors on rack-and-pinion steering meshing', *First World Congress on Condition Monitoring*.

Popov, V.L. (2010) *Contact Mechanics and Friction*, Springer Berlin Heidelberg, Berlin.

Simionescu, P.A. and Smith, M.R. (2000) 'Initial estimates in the design of rack-and-pinion steering linkages', *Journal of Mechanical Design*, Vol. 122, No. 2, pp.194–200.

Spitas, C. and Spitas, V. (2006) 'Calculation of overloads induced by indexing errors in spur gearboxes using multi-degree-of-freedom dynamical simulation', *Proceedings of the Institution of Mechanical Engineers, Part K: Journal of Multi-body Dynamics*, Vol. 220, No. 4, pp.273–282.

Wou, S.J., Oste, T.D. and Baxter, J. (2001) *Modelling of Mesh Friction and Mechanical Efficiency of Rack-and-pinion Steering Design*, No. 2001-01-0485, SAE Technical Paper.

Xue, Y. and Watton, J. (2005) 'Modelling of a hydraulic power steering system', *International Journal of Vehicle Design*, Vol. 38, Nos. 2–3, pp.162–178.

Yao, J. and Angeles, J. (2000) 'The kinematic synthesis of steering mechanisms', *Transactions-Canadian Society for Mechanical Engineering*, Vol. 24, Nos. 3–4, pp.453–476.

Zhang, Y. and Fang, Z. (1999) 'Analysis of tooth contact and load distribution of helical gears with crossed axes', *Mechanism and Machine Theory*, Vol. 34, No. 1, pp.41–57.